Geophysical Prospecting, 2002, **50**, 97–106

Poisson's ratio at high pore pressure

José M. Carcione* and Fabio Cavallini

Istituto Nazionale di Oceanographia e di Geofisica Sperimentale, Borgo Grotta Gigante 42/C, 34010 Sgonico (TS), Italy

Received June 2000, revision accepted May 2001

ABSTRACT

Laboratory investigations suggest that a precise relationship exists between Poisson's ratio, pore pressure and fluid type. Values of Poisson's ratio for dry samples are significantly smaller than those for fluid-saturated samples. The values are anomalously high for high pore pressure, with the possibility of differentiating between gas-saturated, brine-saturated and oil-saturated porous rocks.

The present study considers two overpressure models, based on oil/gas conversion and disequilibrium compaction, to obtain Poisson's ratio versus differential pressure (confining pressure minus pore pressure). The model results are in good agreement with experiments. Poisson's ratio is approximately constant at high differential pressures and increases (decreases) for saturated (dry) rocks at low differential pressures. Fluid type can be determined at all differential pressures from Poisson's ratio. The analysis is extended to the anisotropic case by computing the three Poisson's ratios of a transversely isotropic rock versus differential pressure. While one of them is practically independent of effective pressure, the others increase with increasing pore pressure. Experiments performed on cores under different pressure conditions, and calibration of the models with these data, provide a tool for inverting pore pressure from seismic data.

INTRODUCTION

Knowledge of pore pressure when using seismic data helps in planning the drilling process to control potentially dangerous, abnormally high pressures. One of the parameters most sensitive to rock lithology is Poisson's ratio v, given by

$$v = \frac{1}{2}\left(1 - \frac{1}{a-1}\right), \quad a \equiv \left(\frac{V_P}{V_S}\right)^2, \tag{1}$$

where V_P and V_S are the compressional- and shear-wave velocities. This formula shows clearly that v increases with a. Alternatively, Poisson's ratio may be expressed in terms of elastic parameters as

$$v = \frac{1}{2}\left(1 - \frac{1}{1/3 + K/\mu}\right), \tag{2}$$

where K denotes bulk modulus (a measure of incompressibility) and μ denotes shear modulus. Thus, v increases with the ratio K/μ, and since stability requirements dictate that K and μ be positive, it can also be seen from this formula that $-1 < v < 1/2$. These limits correspond to a solid of very high rigidity ($\mu \to \infty$) and to a fluid ($\mu \to 0$), respectively.

As can be appreciated in Fig. 1, v is sensitive to micropore structure and fluid type (Tatham 1982; Tao, King and Nabi-Bidhendi 1995; Khazanehdari, McCann and Sothcott 1998, paper presented at conference on pressure regimes in sedimentary basins and their prediction, Del Lago resort, Lake Conroe, TX, USA). In samples of equal porosity, it is the aspect ratio of the cracks and pores and the saturating fluid which determine v. Rocks containing mainly round voids (stiff pores) do not show major variations in v with effective stress. Closure of microcracks (compliant pores) will increase the bulk modulus K more than the shear modulus μ, assuming a random distribution of these pores; hence, in dry rocks, Poisson's ratio increases with increasing differential pressure

*E-mail: jcarcione@ogs.trieste.it

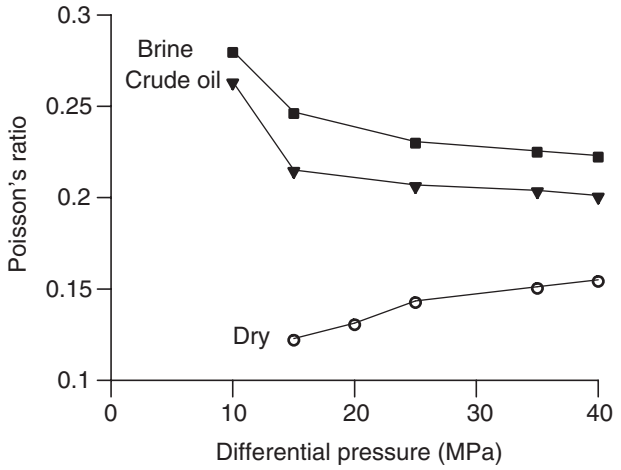

Figure 1 Plot of Poisson's ratio versus differential pressure for different pore-fluid types (Khazanehdari *et al.* 1998, as in text).

(see Fig. 1). In saturated rocks, the compliant pores become stiff, so that Poisson's ratio hardly changes as the pore pressure increases. Laboratory experiments show that v for a dry sample is significantly smaller than that of the fluid-saturated sample. Moreover, v increases with increasing pore pressure and decreasing differential pressure. At zero differential pressure, V_S is zero, because the rock is hydrocracked (and has no rigidity), but V_P is not zero (even for a completely cracked rock), therefore a should be infinite and $v \to 1/2$. Note that v is a function of the ratio of compressional-wave velocity to shear-wave velocity. This relationship removes the effect of the density, eliminating a possible uncertainty. Various physical processes cause anomalous pressures on an underground fluid. The two most common causes are chemical cracking, i.e. oil-to-gas conversion, and non-equilibrium or disequilibrium compaction. Oil-to-gas cracking may increase the pore pressure so that it reaches or exceeds the lithostatic pressure (Luo and Vasseur 1996). Oil can be generated from kerogen-rich source rocks and it can then migrate through a carrier bed to a sandstone reservoir rock. If the reservoir is sealed on all sides by an impermeable shale or limestone, then the condition of a *closed system* will be satisfied for gas generation. Recalling that "much of the oil and gas has been generated from source rocks inside deep (>3000 m or 9840 ft) seal-bounded fluid compartments" (Hunt 1990), we may argue that this condition can be found in most sedimentary basins (Bradley 1975) and, specifically, in the southern North Sea where gas is contained in Rotliegende reservoirs originated from Carboniferous source rocks.

The overpressure model considers a reservoir, initially at hydrostatic pressure, that, due to the sealed condition, develops pore pressures higher than hydrostatic during burial. Carcione and Gangi (2000a) developed a simple model to calculate the excess pore pressure and rock acoustic properties as a function of the fraction of oil converted to gas. In the next section we develop this approach further.

Disequilibrium compaction or mechanical compaction disequilibrium is a consequence of a rapid deposition compared to the time required for expelling the fluids from the pore space by gravitational compaction. In this situation, the fluids carry part of the load that would be held by grain contacts, and abnormal pore pressures develop in the pore space. A description of this mechanism has been given by Rubey and Hubbert (1959). Recently, Carcione and Gangi (2000b) obtained the seismic properties of the rock versus pore and confining pressures. The seismic attributes are calculated using a modification of Biot's theory for partially saturated, porous solids. The mixture gas/oil or oil/brine behaves as a composite fluid with properties depending on the constants of the constituents and their relative concentrations. The bulk modulus is obtained by Wood's averaging, and the density and viscosity by arithmetic averaging (Berryman, Thigpen and Chin 1988).

The main aim of this paper is to investigate the sensitivity of Poisson's ratio to changes in differential pressure and fluid composition, generated by oil-to-gas conversion and non-equilibrium compaction. To this end, the models introduced by Carcione and Gangi (2000a,b) are considered in the next two sections. The analysis of Poisson's ratio is extended in the final section to the anisotropic case, which arises when increasing pore pressure induces a preponderance of crack openings perpendicular to the minimum *in situ* principal stress. The rock can then be approximated by a transversely isotropic medium, with a horizontal symmetry axis if the minimum stress is in the horizontal direction. In this case, three main Poisson's ratios can be defined. Their dependences on confining and pore pressure are obtained using Biot's anisotropic theory (Carcione 1996; Cheng 1997).

OVERPRESSURE DUE TO CRACKING

Let us assume a reservoir at initial depth z_i, with lithostatic confining pressure p_{ci}, hydrostatic pore pressure $p_i = p_{Hi}$ and temperature T_i. The model developed by Carcione and Gangi (2000a) yields, at depth $z > z_i$, the pore pressure p, the confining pressure p_c and the temperature T. The lithostatic pressure at depth z for an average sediment density $\bar{\rho}$ is equal to $p_c = \bar{\rho} g z$, where g is the acceleration due to gravity. The hydrostatic pore pressure is approximately $p_H = \rho_w g z$,

where ρ_w is the density of brine. For a constant sediment burial rate S and a constant geothermal gradient G, the temperature variation of a particular sediment volume is $T = T_0 + Gz$, where $z = St$, with a surface temperature T_0 at time $t = 0$.

The mass of convertible oil changes with time t at a rate proportional to the mass itself. Assuming a first-order kinetic reaction (Luo and Vasseur 1996; Berg and Gangi 1999) and a reaction rate following the Arrhenius equation, it can be shown that the oil-to-gas conversion factor is given by

$$F(T) = 1 - \exp[\Psi(T_i) - \Psi(T)], \tag{3}$$

with

$$\Psi(T) = \frac{A}{H}\frac{T\exp[-E/(RT)]}{2 + E/(RT)}, \tag{4}$$

where A is the oil–gas reaction rate at infinite temperature, $H = GS$, R is the gas constant, T_i is the initial temperature and E is the activation energy (Carcione and Gangi 2000a).

The excess pore pressure at depth z is $p - p_H$, where p is the pore pressure when a fraction F of oil has been converted to gas ($F = 0$ and $p = p_i = p_H$ at time t_i). In general, compressional- and shear-wave velocities depend on the effective pressure $p_e = p_c - np$, where $n \leq 1$ is the effective-stress coefficient. Note that the effective pressure equals the confining pressure at zero pore pressure. It is found that $n \approx 1$ for static measurements of the compressibilities (Zimmerman, Somerton and King 1986), while n is approximately linearly dependent on the differential pressure $p_d = p_c - p$ in dynamic experiments (Gangi and Carlson 1996; Prasad and Manghnani 1997):

$$n = n_0 - n_1 p_d, \tag{5}$$

where the coefficients n_0 and n_1 are constant. The concept of an effective-stress coefficient is implicit in the stress–strain relationships of Biot's theory, corresponding to static bulk deformations (Todd and Simmons 1972).

We assume the following functional form for the pore compressibility c_p as a function of effective pressure p_e:

$$c_p = c_p^\infty + \beta \exp\left(-\frac{p_e}{p^*}\right), \tag{6}$$

where c_p^∞, β and p^* are coefficients obtained by fitting the experimental data. This function describes very accurately the compressibility c_p as a function of the effective pressure p_e (Zimmerman *et al.* 1986), and the same functional dependence relates wet-rock ultrasonic velocities to effective pressure (Prasad and Manghnani 1997).

We assume that the medium is fully saturated with oil and that, before oil/gas conversion occurs, the initial pressure p_i is hydrostatic. Equating mass and volume fractions in the pore space yields the relationship between the oil-to-gas conversion factor F and the pore pressure p (Carcione and Gangi 2000a):

$$F = \frac{\exp[E(\Delta p) + \alpha_p \Delta T] - \exp(-c_o \Delta p + \alpha_o \Delta T)}{\rho_o/\rho_g(p,T) - \exp(-c_o \Delta p + \alpha_o \Delta T)}, \tag{7}$$

where

$$E(\Delta p) = -c_p^\infty \Delta p_e + \beta p^* \left[\exp\left(-\frac{p_e}{p^*}\right) - \exp\left(-\frac{p_{ei}}{p^*}\right)\right], \tag{8}$$

ρ_o is the oil density and ρ_g is the gas density at depth z, obtained from the van der Waals equation, c_o is the oil compressibility, α_o is the thermal expansion of oil, $\Delta p = p - p_i$ is the pore-pressure increase, $\Delta p_e = p_e - p_{ei}$ is the effective pressure increase ($p_{ei} = p_{ci} - np_i$), $\Delta T = T - T_i$ is the temperature increase and α_p is the thermal expansion of the pore space.

With a surface temperature of 25 °C, a temperature gradient G of 25 °C/km, a sedimentation rate S of 0.08 km/m.y. (m.y.: million years) and a reservoir at depth $z_i = 2$ km, we obtain t_i = 25 m.y. and $T_i = 75$ °C. After 75 m.y., the depth of burial is 8 km, geological time is 100 m.y. and the temperature is 225 °C. On the other hand, if $\bar{\rho} = 2400\,\text{kg/m}^3$, the confining pressure has increased from 47 MPa to approximately 188 MPa and the initial pore pressure is $p_i \simeq 20$ MPa (assuming $\rho_w = 1000\,\text{kg/m}^3$). If no conversion takes place, the final pore pressure would be the hydrostatic pressure at 8 km, i.e. approximately 78 MPa. We assume that the generated gas does not go into solution in the oil. It has been shown by Carcione and Gangi (2000a) that if this happens the results are practically the same, since the volume increase of the live oil is close to that of the dead oil/free gas mixture.

The experimental data for oil-saturated sandstone are available in Winkler (1985) (note that Winkler calls the differential pressure the effective stress). The experiments on dry samples correspond to zero pore pressure. Best-fit approximations of the dry-rock compressibility and shear modulus versus confining pressure are

$$K_m^{-1}[\text{GPa}^{-1}] = 0.064 + 0.122\exp\left(-\frac{p_c[\text{MPa}]}{6.48}\right) \tag{9}$$

and

$$\mu_m[\text{GPa}] = 13.7 - 8.5\exp\left(-\frac{p_c[\text{MPa}]}{9.14}\right), \tag{10}$$

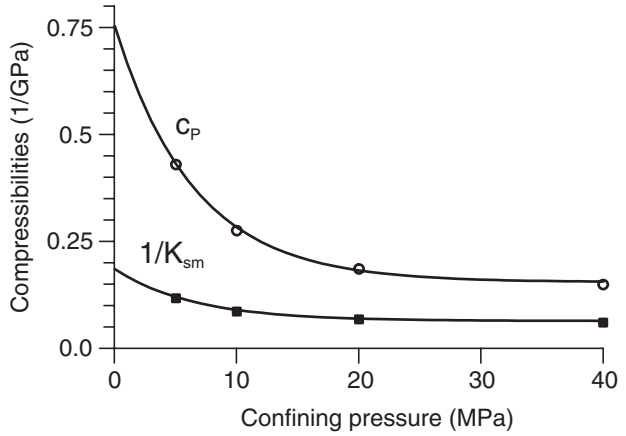

Figure 2 Best-fit plots of pore compressibility c_p and matrix compressibility K_m^{-1} obtained from the experimental data for Berea sandstone published by Winkler (1985, Figs 3 and 4, Tables 4 and 7).

and c_p in Gpa^{-1} is given by (6), with $c_p^\infty = 0.155\,\text{GPa}^{-1}$, $\beta = 0.6\,\text{GPa}^{-1}$ and $p^* = 6.48$ MPa. The pore compressibility c_p has been obtained from the dry-rock bulk modulus by assuming that the porosity is that at hydrostatic pore pressure. The best-fit plots for c_p and K_m^{-1} are shown in Fig. 2.

In order to obtain the moduli for different combinations of the confining and pore pressures, we make the substitution $p_c \rightarrow p_e = p_c - n(p_H + \Delta p)$, where we assume, following Gangi and Carlson (1996), that n depends on differential pressure according to (5) with $n_0 = 1$ and $n_1 = 0.014\,\text{MPa}^{-1}$. This dependence of n on differential pressure is in good agreement with the experimental values corresponding to the compressional-wave velocity obtained by Prasad and Manghnani (1997).

Table 1 indicates the properties for Berea sandstone and the different fluids, with the values corresponding to those at the initial (hydrostatic) pore pressure. The oil density and oil bulk modulus are assumed to be pressure independent. The oil and gas viscosities (η_o and η_g) as a function of temperature and pore pressure are taken from Luo and Vasseur (1996). Other properties required by Biot's theory are the grain density ρ_s, the grain bulk modulus K_s, the grain rigidity μ_s, the brine viscosity η_w, the rock porosity ϕ and the rock permeability κ.

Although (3) and (4) indicate that the high activation energy requires either a long time to elapse or deep burial, of the order of 4.5 to 5 km, before appreciable fractions of conversion occur, significant fractional conversions occur at 3 km. The pore-pressure build-up with depth is shown in Fig. 3. The pressure rapidly increases for very small fractions of oil converted to gas; after approximately 4% conversion,

Table 1 Rock properties

Grain	$\rho_s = 2650\,\text{kg/m}^3$
	$K_s = 37\,\text{GPa}$
	$\mu_s = 39\,\text{GPa}$
Oil	$\rho_o = 700\,\text{kg/m}^3$
	$K_o = 0.57\,\text{GPa}$
	$\alpha_o = 5 \times 10^{-4}\,^\circ\text{C}^{-1}$
	$\eta_o = 440\,\text{cP}$
Gas	$\eta_g = 0.012\,\text{cP}$
Water	$\rho_w = 1040\,\text{kg/m}^3$
	$K_w = 2.25\,\text{GPa}$
	$\alpha_w = 7.7 \times 10^{-4}\,^\circ\text{C}^{-1}$
	$\eta_w = 1.8\,\text{cP}$
Matrix	$K_m = 15.45\,\text{GPa}$
	$\mu_m = 13.48\,\text{GPa}$
	$\phi = 0.203$
	$\kappa = 10^{-12}\,\text{m}^2$
	$\alpha_p = 3 \times 10^{-4}\,^\circ\text{C}^{-1}$

$1\,\text{cP} = 0.001\,\text{Pa s}$.

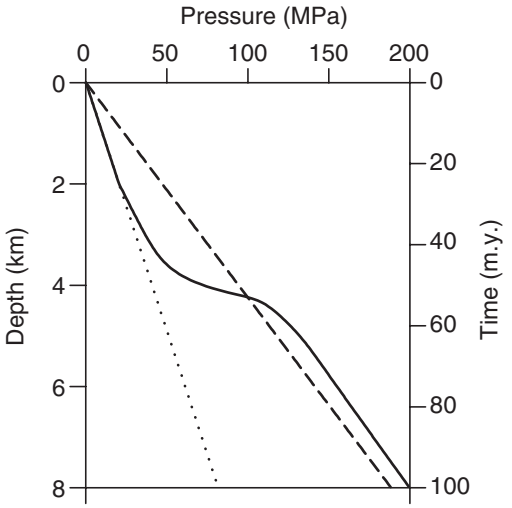

Figure 3 Pore-pressure build-up with depth and deposition time (continuous line). The hydrostatic and lithostatic pressure are represented by dotted and broken lines, respectively.

the pore pressure equals the confining pressure. The pore-pressure curve has no physical meaning for values exceeding the confining pressure (in this case, below 4.2 km depth), since the reservoir is fractured by the excess pore pressure and the fluid is released. The model does not take this process into account.

Curves of low-frequency Poisson's ratio versus differential pressure, obtained from Biot's theory (Berryman *et al.* 1988;

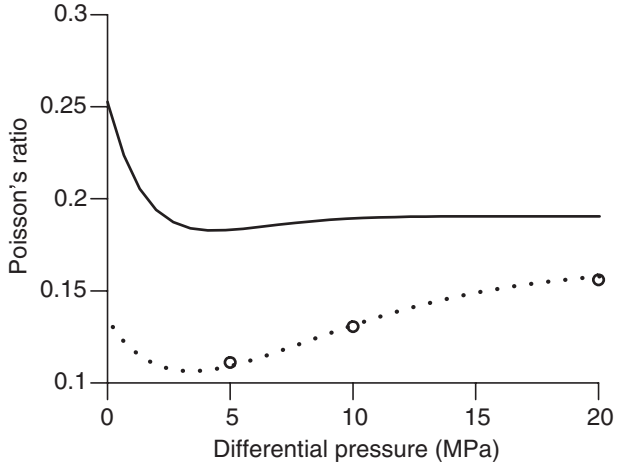

Figure 4 Poisson's ratio versus differential pressure for overpressure due to cracking. The continuous line corresponds to the rock saturated with oil and gas, and the dotted line corresponds to the dry rock (the open circles are experimental values for the dry rock).

Carcione and Gangi 2000a,b), are shown in Fig. 4. The continuous line corresponds to the rock saturated with oil and gas, and the dotted line to the dry rock. The open circles are the experimental values of Poisson's ratio. According to Gassmann's equation (e.g. Mavko, Mukerji and Dvorkin 1998), the bulk modulus is higher in saturated rocks than in dry ones; and the same is then true for Poisson's ratio, according to (2). Our model also predicts a higher v for the saturated rock, mainly at low differential pressures, i.e. at very high pore-fluid pressures. In the saturated case at low differential pressures, v increases with increasing pore pressure (i.e. decreasing differential pressure), since the pore fluid opens the compliant pores (microcracks). Conversely, in the dry case the microcracks close with increasing confining pressure, since the pore pressure vanishes.

ABNORMAL PRESSURE DUE TO DISEQUILIBRIUM COMPACTION

The case of non-equilibrium compaction is that in which the sedimentation rate is so rapid that the pore fluids do not have a chance to 'escape'. We assume that the pore space is filled with organic material and brine, and that the compressibilities of the organics and brine are independent of pressure and temperature, while the compressibility of the rock is independent of temperature but is dependent on pressure. At the initial time t_i, corresponding to depth z_i, the volume of rock behaves as a closed system. It can be shown that by equating mass and volume fractions in the pore space (Carcione and Gangi 2000b), we obtain

$$\exp[E(\Delta p) + \alpha_p \Delta T] = S_{wi} \exp(-c_w \Delta p + \alpha_w \Delta T) + (1 - S_{wi}) \exp(-c_o \Delta p + \alpha_o \Delta T), \quad (11)$$

where S_{wi} denotes the initial brine saturation, c_w denotes brine compressibility and α_w denotes thermal expansion of brine.

The solution of (11) gives the pore pressure p as a function of depth and deposition time, with $\Delta T = T - T_i = G(z - z_i) = GS(t - t_i)$ for a constant geothermal gradient and a constant sediment burial rate.

The dry-rock moduli for the sandstone are those given by Winkler (1985), illustrated in the previous example (Table 1 also indicates the properties for brine). The pore-pressure profiles with depth for $S_w = 0$ (label 1), $S_w = 0.5$ (label 2) and $S_w = 1$ (label 3), are shown in Fig. 5, where the continuous lines represent the hydrostatic and lithostatic pressures. The rock is underpressured for full oil saturation, and increasing brine saturation implies overpressure. The pore-pressure profile depends on the compressibility and thermal expansion coefficient of the mixture filling the pore space. Rocks saturated with fluids of high compressibility and low thermal expansion coefficient are generally underpressured, and rocks saturated with fluids of low compressibility and high thermal expansion coefficient are generally overpressured, and can be seismically 'visible' (Carcione and Gangi 2000b).

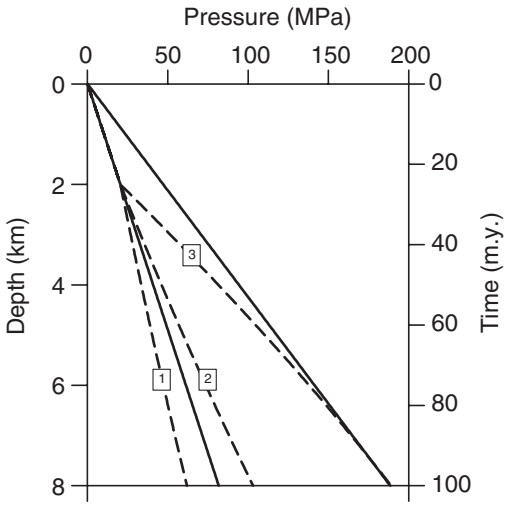

Figure 5 Pore-pressure build-up with depth and deposition time for full oil saturation ($S_w = 0$, label 1), 50% oil saturation ($S_w = 0.5$, label 2) and full brine saturation ($S_w = 1$, label 3). The hydrostatic and lithostatic pressures are represented by continuous lines.

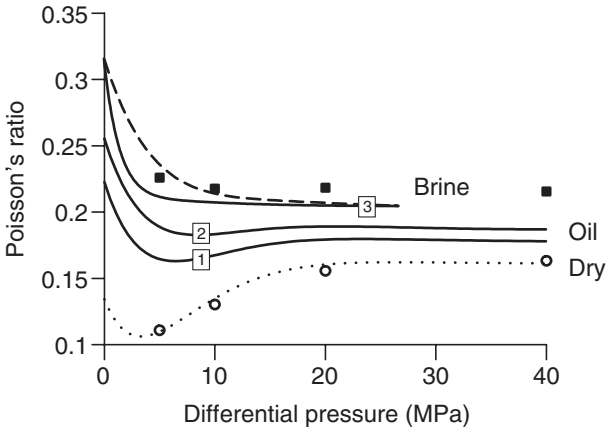

Figure 6 Poisson's ratio versus differential pressure for disequilibrium compaction. The open circles and black squares are the experimental values for the oil-saturated and dry samples, obtained from Winkler's (1985) data. The curves correspond to the cases indicated in Fig. 5. In the case of full brine saturation (label 3), the broken line corresponds to the range 0 to 2 km, where the rock is normally pressured, and the continuous lines correspond to the range 2 to 8 km, where the rock is overpressured.

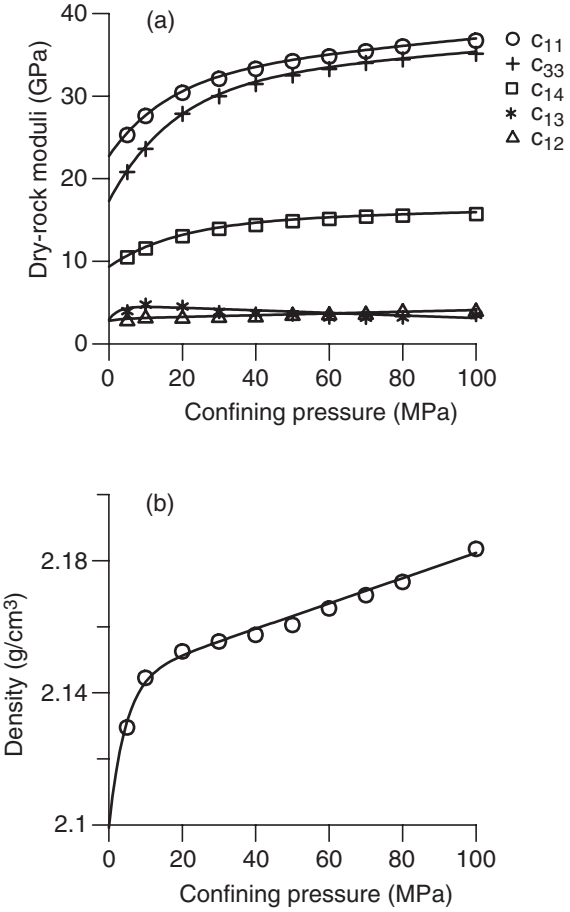

Figure 7 Best-fit curves to (a) the dry-rock elastic constants and (b) the density of Berea sandstone versus confining pressure p_c. The experimental data are from Lo *et al.* (1986).

Figure 6 shows Poisson's ratio versus differential pressure, where the open circles and black squares are the experimental values for the dry and oil-saturated samples, obtained from Winkler's data. The curve labelled 2 corresponds to saturation with 50% oil and 50% brine. This curve, the broken line for brine (label 3) and that for oil (label 1) correspond to the range from 0 to 2 km at low differential pressure, where the rock is normally pressured. The pore pressure approaches the confining pressure at very shallow depths, and the effect is exactly equivalent to that caused by overpressuring at great depths, which is represented by the continuous line for brine. The curves have the same qualitative behaviour as in the case of overpressure due to cracking. Moreover, Poisson's ratio increases with increasing brine saturation. The discrepancies between the experimental values and curve 1 (full oil saturation) are due to the fact that Winkler's oil compressibility (2.16 GPa) is closer to brine compressibility (2.25 GPa) than the value used in this work (0.57 GPa). In fact, the points are close to the Poisson's ratio for full brine saturation.

The model could be improved by considering the fact that the compressibility of oil depends on pressure and temperature. This is, however, a second-order effect. Indeed, the results given by Batzle and Wang (1992) in their Figs 5 and 13 show that the density is almost a linear function of temperature and pressure. This means that the above-mentioned properties are approximately constant (see also Batzle and Wang's (1992) Fig. 7, where the oil compressibility remains almost constant when changing from low temperature and low pressure to high temperature and high pressure). Another influencing factor is the presence of dissolved gas in the oil. However, Carcione and Gangi (2000a) have shown that this factor is not important at the depth under consideration.

OVERPRESSURE IN ANISOTROPIC ROCKS

A rock in the subsurface is subjected to a non-hydrostatic state of stress: in general, the vertical stress is greater than the horizontal stress, and this situation induces P- and S-wave anisotropy in an otherwise isotropic rock. A proper analysis of the dependence of Poisson's ratio on pore pressure and confining stress in anisotropic media requires a complete experimental data set, i.e. dry-rock velocity measurements

versus confining stress, and wet-rock velocity measurements versus pore pressure and confining stress. In addition, the density is required for simulating wave propagation. A complete data set is, to our knowledge, not yet available in the literature. We consider the dry-rock measurements in transversely isotropic Berea sandstone obtained by Lo, Coyner and Toksöz (1986) and obtain the effective stress coefficient from Biot's poro-elastic theory. Although Lo *et al.*'s (1986) data do not reflect the situation at depth, since their sample is anisotropic at zero confining pressure and they applied an isotropic confining stress, the results of the pore-pressure analysis should, in principle, be equivalent to those obtained from an anisotropic stress applied to an isotropic rock.

Figure 7 shows the best-fit curves to the dry-rock elastic constants (a) and density (b) of Berea sandstone versus confining pressure p_c. We obtain

$$\begin{aligned} c_{11} &= 32.74 + 0.043\,p_c - 9.97\exp(-0.06\,p_c),\\ c_{33} &= 31.87 + 0.035\,p_c - 14.59\exp(-0.056\,p_c),\\ c_{44} &= 14.93 + 0.011\,p_c - 5.58\exp(-0.053\,p_c),\\ c_{12} &= 3.06 + 0.01\,p_c - 0.26\exp(-0.25\,p_c),\\ c_{13} &= 4.68 - 0.015\,p_c - 1.7\exp(-0.036\,p_c),\\ \rho &= 2144.1 + 0.38\,p_c - 45\exp(-0.0226\,p_c), \end{aligned} \tag{12}$$

where the elastic constants are given in GPa, the density in kg/m^3 and the confining pressure in MPa. Polar representations of the dry-rock energy velocities are shown in Figs 8(a,b) for $p_c = 0$ MPa and $p_c = 100$ MPa, respectively. The curves correspond to a plane perpendicular to the plane of isotropy. Only one-quarter of the curves are shown, because of symmetry considerations. The tick marks indicate the polarization directions, with the points uniformly sampled as a function of the phase angle (the symbol 'q' is an abbreviation for 'quasi': indeed, the polarization is neither exactly perpendicular nor exactly parallel to the energy velocity section). The energy velocities are calculated by using the anisotropic poro-elastic stress–strain relationships (Cheng 1997), and by computing the eigenvalues of the Christoffel matrix. The whole procedure for the 2D case has been given by Carcione (1996). Note that, as expected, the wavefronts are more anisotropic at zero confining pressure.

Three dynamic Poisson's ratios, corresponding to different directions can be obtained. Assume that the axis of symmetry coincides with the z-axis, and denote the strain along the Cartesian axes by ε_{xx}, ε_{yy} and ε_{zz}. Then the different Poisson's ratios are (Lo *et al.* 1986)

$$v_1 = \frac{\varepsilon_{yy}}{\varepsilon_{xx}} = \frac{c_{12}c_{33} - c_{13}^2}{c_{11}c_{33} - c_{13}^2}, \tag{13}$$

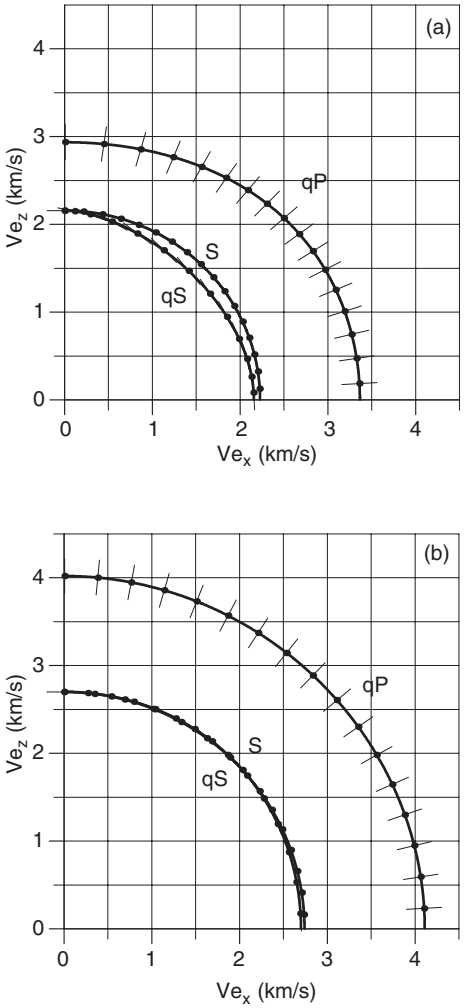

Figure 8 Polar representations of the dry-rock energy velocities for (a) $p_c = 0$ MPa and (b) $p_c = 100$ MPa. The curves correspond to a plane perpendicular to the plane of isotropy. Only one-quarter of the curves are shown because of symmetry considerations. The tick marks indicate the polarization directions.

$$v_2 = \frac{\varepsilon_{zz}}{\varepsilon_{xx}} = \frac{c_{13}(c_{11} - c_{12})}{c_{11}c_{33} - c_{13}^2}, \tag{14}$$

if the sample is compressed along the x-direction, and

$$v_3 = \frac{\varepsilon_{xx}}{\varepsilon_{zz}} = \frac{c_{13}}{c_{11} + c_{12}}, \tag{15}$$

if the sample is compressed along the symmetry axis. These Poisson's ratios all tend to v when the medium is isotropic ($c_{11} = c_{33} = c_{12} + 2c_{44} = \rho V_P^2, \quad c_{12} = c_{13} = \rho(V_P^2 - 2V_S^2)$). Equations (13), (14) and (15) also give the expressions for the wet-rock Poisson's ratios.

We consider a sandstone at depth $z = 3$ km. If the average sediment density is 2400 kg/m^3, the confining pressure is

$p_c = 70.6$ MPa and the hydrostatic pressure is $p_H = 30.6$ MPa (assuming $\rho_w = 1040\,\mathrm{kg/m^3}$). With a surface temperature of 25 °C and a geothermal gradient $G = 25\,^\circ\mathrm{C/km}$, we have a temperature $T = 100\,^\circ\mathrm{C}$.

In order to calculate the wet-rock Poisson's ratios versus pore and differential pressure, we must obtain the density and elastic constants as a function of effective stress. The concept of effective stress is implicit in Biot's theory. Hooke's law (in Voigt notation) for anisotropic poro-elastic media can be written as

$$\tau_I = c_{IJ}\varepsilon_J - n_I p, \qquad I,J = 1,\ldots,6, \tag{16}$$

where τ_I is the total stress vector, ε_J is the strain vector of the porous frame and n_I are the effective stress coefficients (Cheng 1997). In this context, the effective stress is given by $\tau_{eI} = c_{IJ}\varepsilon_J$, such that

$$\tau_{eI} = \tau_I + n_I p. \tag{17}$$

For transversely isotropic media, $n_1 = n_2$ and $n_4 = n_5 = n_6 = 0$. It is clear that no single pore pressure value implies $c_{IJ}\varepsilon_J = 0$ for a hydrostatic confining stress $\tau_I = -p_c$, $I = 1,2,3$. An approximation is to assume an average effective stress coefficient,

$$n = \frac{2n_1 + n_3}{3}, \tag{18}$$

and an effective pressure $p_e = p_c - np$. In this case $(c_{1J} + c_{2J} + c_{3J})\varepsilon_J = 0$. Then, the elastic constants of the frame versus pore and confining pressures are obtained from (12) by substituting p_c with p_e, and the wet-rock elastic constants are obtained from the stress–strain relationship provided by Cheng (1997). As before, the energy velocities follow from the plane-wave theory developed by Carcione (1996). Polar representations of the wet-rock energy velocities are shown in Figs 9(a,b) for $p = 5$ MPa and $p = 100$ MPa, respectively. The saturating fluid is brine. At high pore pressure (microcracks open) the medium shows a higher degree of anisotropy than at low pore pressure. Finally, Fig. 10 shows Poisson's ratio versus effective pressure for the rock saturated with brine, oil and gas, compared with the dry-rock Poisson's ratios. While ν_1 is practically independent of effective pressure, ν_2 and ν_3 increase with decreasing effective pressure (increasing pore pressure). The effect is important and therefore the determination of these Poisson's ratios enables us to monitor abnormal pore-pressure conditions. It is clear, as in the isotropic case, that it is possible to distinguish between different saturating fluids using Poisson's ratio as a diagnostic parameter.

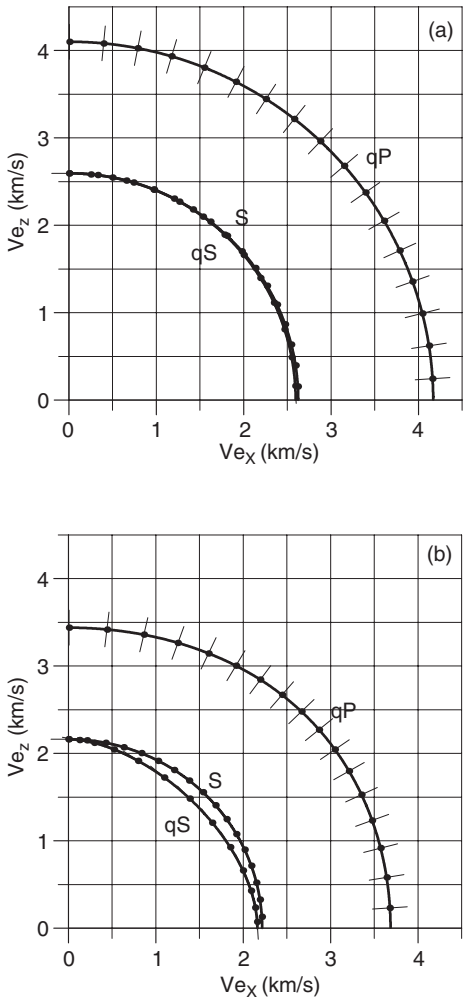

Figure 9 Polar representations of the wet-rock energy velocities for (a) $p = 0$ MPa and (b) $p = 100$ MPa. The saturating fluid is brine. The curves corresponds to a plane perpendicular to the plane of isotropy. Only one-quarter of the curves are shown because of symmetry considerations. The tick marks indicate the polarization directions.

CONCLUSIONS

Laboratory measurements of wave velocities versus confining and pore pressures give the relationships between Poisson's ratio and the *in situ* conditions (fluid composition, pore pressure, etc.) of reservoir rocks, offering a basis for physical and geological insight into the lithological interpretation of seismic data.

The variations in Poisson's ratio have been determined as a function of excess pressure due to oil/gas conversion and disequilibrium compaction. In the first case, Poisson's ratio increases significantly when only a small amount (about 4%) of the oil is converted to gas. The effective pressure decreases

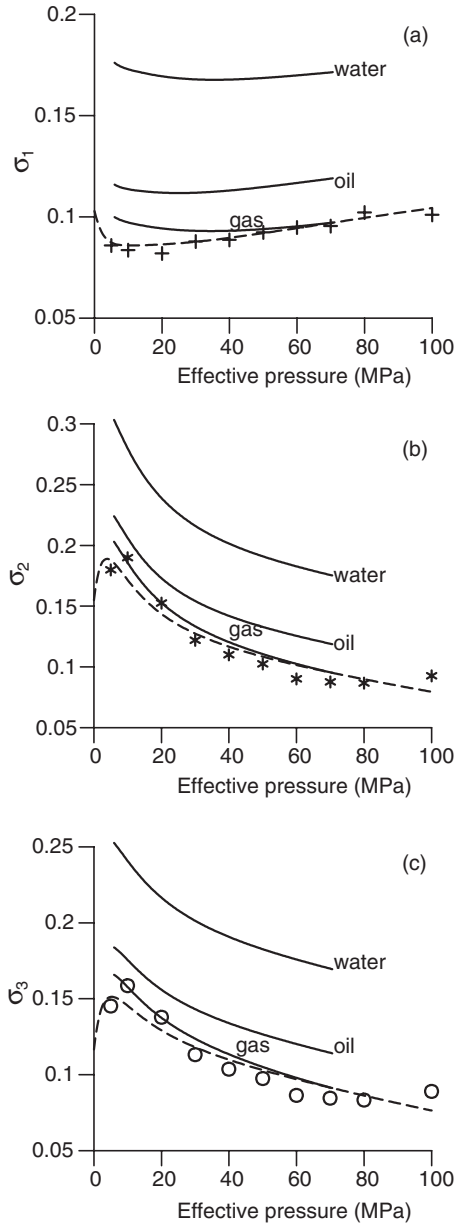

Figure 10 Anisotropic Poisson's ratios (a) $\sigma_1 = \nu_1$, (b) $\sigma_2 = \nu_2$ and (c) $\sigma_3 = \nu_3$, for brine-, oil- and gas-saturated Berea sandstone versus effective pressure, compared with the experimental dry-rock Poisson's ratios (Lo *et al.* 1986). The dashed line is the best-fit curve to the dry-rock data.

since the pore pressure increases due to the conversion of the high-density oil to the low-density gas. The case of disequilibrium compaction shows that the fluid mixture filling the pore space has a major influence on Poisson's ratio and may cause underpressure or overpressure, depending on its compressibility. In fact, full oil saturation in the pore space implies a pore pressure lower than hydrostatic pressure. For rocks under *in situ* conditions, Poisson's ratio increases as the differential pressure approaches zero. On the other hand, the isotropic dry-rock Poisson's ratio, obtained at zero pore pressure, decreases with decreasing differential (confining) pressure, but the effect is important at very low differential pressures. The situation is different when anisotropy is taken into account. In this case, two of the three (dry- and wet-rock) Poisson's ratios increase with decreasing effective pressure, and the effect is important at all effective pressures.

Using Poisson's ratio as a diagnostic parameter of pore pressure requires laboratory experiments on cores taken from a well in the area of study. To summarize:

1 Obtain the dry-rock moduli versus confining pressure. This gives the dependence of these moduli on effective pressure, and implicitly includes microstructural information, such as the effects of closing of compliant cracks.

2 Perform experiments on saturated samples for different confining and pore pressures, in order to obtain the effective stress coefficient n. Alternatively, n can be approximately estimated from Biot's theory.

3 Compute the wave velocities and Poisson's ratio for different fluid compositions and saturations versus pore and confining pressure.

4 Identify the abnormal pressure mechanism in the area.

5 Use the proposed models to invert for pore pressure from seismic and available well data.

It appears that the results of the present work have potential applications to rock physics (e.g. anisotropic properties), petroleum engineering (overpressure prediction while drilling) and geophysical interpretation (fluid-type recognition).

ACKNOWLEDGEMENTS

This work was partly supported by the European Union under the project 'Detection of overpressure zones with seismic and well data'. Helpful remarks from the Associate Editor, G. Diephuis, are gratefully acknowledged.

REFERENCES

Batzle M. and Wang Z. 1992. Seismic properties of pore fluids. *Geophysics* **57**, 1396–1408.

Berg R.R. and Gangi A.F. 1999. Primary migration by oil-generation microfracturing in low-permeability source rocks: application to the Austin chalk, Texas. *Bulletin of the American Association of Petroleum Geologists* **83**, 727–756.

Berryman J.G., Thigpen L. and Chin R.C.Y. 1988. Bulk elastic wave propagation in partially saturated porous solids. *Journal of the Acoustical Society of America* **84**, 360–373.

Bradley J.S. 1975. Abnormal formation pressure. *Bulletin of the American Association of Petroleum Geologists* **79**, 957–973.

Carcione J.M. 1996. Wave propagation in anisotropic, saturated porous media: plane wave theory and numerical simulation. *Journal of the Acoustical Society of America* **99**, 2655–2666.

Carcione J.M. and Gangi A.F. 2000a. Gas generation and overpressure: effects on seismic attributes. *Geophysics* **65**, 1769–1779.

Carcione J.M. and Gangi A.F. 2000b. Non-equilibrium compaction and abnormal pore-fluid pressures: effects on seismic attributes. *Geophysical Prospecting* **48**, 521–537.

Cheng A.H.-D. 1997. Material coefficients of anisotropic poroelasticity. *International Journal of Rock Mechanics, Mineral Science and Geomechanics Abstracts* **34**, 199–205.

Gangi A.F. and Carlson R.L. 1996. An asperity-deformation model for effective pressure. *Tectonophysics* **256**, 241–251.

Hunt J.M. 1990. Generation and migration of petroleum from abnormally pressured fluid compartments. *Bulletin of the American Association of Petroleum Geologists* **74**, 1–12.

Lo T.W., Coyner K.B. and Toksöz M.N. 1986. Experimental determination of elastic anisotropy of Berea sandstone, Chicopea shale, and Chelmsford granite. *Geophysics* **51**, 164–171.

Luo X. and Vasseur G. 1996. Geopressuring mechanism of organic matter cracking: numerical modeling. *Bulletin of the American Association of Petroleum Geologists* **80**, 856–874.

Mavko G., Mukerji T. and Dvorkin J. 1998. *The Rock Physics Handbook*. Cambridge University Press.

Prasad M. and Manghnani M.H. 1997. Effects of pore and differential pressure on compressional wave velocity and quality factor in Berea and Michigan sandstones. *Geophysics* **62**, 1163–1176.

Rubey W.W. and Hubbert M.K. 1959. Role of fluid pressure mechanics of overthrust faulting, II. Overthrust belt in geosynclinal area of Western Wyoming in light of fluid pressure hypothesis. *Bulletin of the Geological Society of America* **70**, 167–205.

Tao G., King M.S. and Nabi-Bidhendi M. 1995. Ultrasonic wave propagation in dry and brine-saturated sandstones as a function of effective stress: laboratory measurements and modelling. *Geophysical Prospecting* **43**, 299–327.

Tatham R.H. 1982. V_P/V_S and lithology. *Geophysics* **47**, 336–344.

Todd T. and Simmons G. 1972. Effect of pore pressure on the velocity of compressional waves in low-porosity rocks. *Journal of Geophysical Research* **77**, 3731–3743.

Winkler K.W. 1985. Dispersion analysis of velocity and attenuation in Berea sandstone. *Journal of Geophysical Research* **90**, 6793–6800.

Zimmerman R.W., Somerton W.H. and King M.S. 1986. Compressibility of porous rocks. *Journal of Geophysical Research* **91**, 12765–12777.